Desalination and Water Treatment
www.deswater.com
doi: 10.1080/19443994.2013.792491

51 (2013) 7746–7763
December

Taylor & Francis
Taylor & Francis Group

Sustainable removal of Cu^{2+}, Ni^{2+} and Zn^{2+} ions from severe contaminated water using kaolin/poly(glycine) composites, characterization and uptake studies

Mohamed A. Mekewi, Atef S. Darwish*, Mohamed E. Amin, Halla A. Bourazan

Department of Chemistry, Faculty of Science, Ain Shams University, Abbassia, 11566 Cairo, Egypt
Tel. +202 24831836; Fax: +202 24831836; email: atef_mouharam@sci.asu.edu.eg

Received 29 August 2012; Accepted 16 March 2013

ABSTRACT

Kaolinite clay of Saint Catharine, Sinai, was treated by glycine molecules and then modified by various diamino-compounds like ethylenediamine, phenyl hydrazine and polyoxypropylenediamine. The native and modified clays were structurally and texturally characterized by XRD, FTIR, XRF, BET, pore size distribution and SEM in addition to exchange capacity parameters. Phenyl hydrazine and polyoxypropylenediamine organo-modifiers proved superior in function compared to ethylenediamine with regard to *in situ* glycine polymerization forming large fragments of ordered polypeptides which acted as super clay sheet binders. Adsorption of Cu(II), Ni(II) and Zn(II) ions by the modified kaolinite under variable concentrations of metal ions and interacting time were studied. Adsorption isotherm investigation indicated that Freundlich equation was a better fit than Langmuir model reflecting surfaces of various accommodated active sites with analogue sites distribution. The adsorption rate constants sequence for all modified kaolinite derivatives proved to be Zn^{2+}>Ni^{2+}>Cu^{2+}. Near 100% removal for Cu^{2+}, Ni^{2+} and Zn^{2+} ions from contaminated water were performed via phenyl hydrazine and polyoxypropylenediamine modified kaolin/poly(glycine) composites due to the expected feature of layers expansion and ultimate exposure of hidden adsorption sites buried deeply in kaolinite interlayers.

Keywords: Sinai kaolinite; Phenyl hydrazine; Polyoxypropylenediamine; Kaolin/poly(glycine) composite; Percentage removal

1. Introduction

Kaolinite is one of the most representative mineral of the four polymorphs in phyllosilicate subclass of general chemical formula Al_2O_3 $2SiO_2$ $2H_2O$. Kaolinite is 1:1 layer silicates consist of a tetrahedral silica sheet and an octahedral alumina sheet bonded together by the sharing of oxygen atoms between zsilicon and aluminium atoms in adjacent sheets, where the 1:1 layers are held together in its crystal form through hydrogen bonding. Accordingly, the kaolinite surfaces (basal faces and edges) have a complex chemistry, since several type of active sites have been cited in kaolinite clays, viz., (i) Brønsted acid sites, created by interlayer water molecules, (ii) Lewis acid sites occurring due to dehydroxylation by thermal treatment [1], (iii) negative charged sites as a

*Corresponding author.

result of isomorphic replacement of Si(IV) by Al(III) atoms in the tetrahedral sheet or of Al(III) by divalent ions (such as Fe(II) and Mg(II)) in the octahedral sheet, (iv) small number of cation exchangeable sites, ranged between 3 and 15 mequiv./100g_{clay}, which are mostly located on the surface of kaolinite rather than the interlayer exchange sites [2,3] and (v) surface hydroxyl groups, mostly found in the edges, bound to Si(IV) or Al(III) cations and occupy approximately 10% of the whole kaolinite surfaces [4,5].

Growing concern about the quality of the natural environment has simulated increasing interest in the physicochemical characteristics and adsorptive behaviour of kaolinite clay as being the most abundant phyllosilicate in highly weathered tropical soils, as well in ocean sediments [6,7]. Kaolinite is considered superior to other phyllosilicate clays such as bentonite and montmorillonite being an ideal surface linear material that is containing (i) small number of surface exchange sites with no interlayer exchange sites [3], (ii) fine aggregates with larger particle size and more irregular particle arrangement that possess low swelling potential, low susceptibility to desiccation and interlayer expansion and low mechanical properties [8]. In turn, much more attention was being paid to modify kaolinite surfaces through acid activation [9,10], thermal treatment [11], mechanochemical activation [12], organo-functionalization [13–15] and recently clay composites [16].

Among the kaolin organo-modifiers, the amino acids (e.g. aspartic acid and glutamic acid), carboxylic acids, and hydroxyacids are promising ligands that enhance the adsorption of metal ion through forming negatively charged surface complexes bridging the metal ions with clay surface [17,18]. Kaolin modification via composite formation were restricted on development of kaolin/poly(olefinic) composites [16] ignoring kaolin/poly(condensate) ones, which may be more valuable in adsorption processes related to their peptide group populations standing for the metal ions complexation.

Although copper, nickel and zinc metal ions are essential nutrients for living organisms, their existence in high concentrations make them, however, outstanding threat to the environmental earth metabolic systems. Gastrointestinal distress, irritating respiratory tract and Wilson's disease were the most commonly reported adverse health effects of copper, [19]. Chronic bronchitis, reduced lung function, allergy and cancer of the lung and nasal sinus were consequences of Ni(II) contamination [20]. Zinc supplementation in healthy adults with high doses resulted in the impairment of various immune responses, pulmonary distress, fever, chills and gastroenteritis [21].

In the present work, glycine molecules, as smallest universe amino acid, were chosen to be the entering agent and various organo-diamine-modifiers such as ethylenediamine, phenylhydrazine and polyoxopropylenediamine were used to improve glycine polymerization within kaolinite layers. The physicochemical properties of diamino-modified kaolin/poly(glycine) composites were also tackled, and the investigation of the solid adsorptive availability toward inorganic pollutants coexisted in severe contaminated water environments had also to be attended.

2. Materials and methods

2.1. Chemicals

Glycine hydrochloride, phenyl hydrazine, ethylenediamine and polyoxopropylenediamine were Aldrich products. Copper(II) nitrate, Nickel(II) nitrate and Zinc (II) nitrate were all supplied by Riedel-De Haen products, Germany. A stock solution of each metal: Ni^{2+} (15,010 ppm), Zn^{2+} (14,590 ppm) and Cu^{2+} (19,415 ppm), is prepared by dissolving $Ni(NO_3)_2.6H_2O$, $Zn(NO_3)_2.6H_2O$ and $Cu(NO_3)_2.3H_2O$, respectively in distilled water.

2.2. Clay adsorbents

Kaolinite clay was collected from Saint Catharine valley, Sinai, Egypt and was sieved to 200 mesh size and dried at 110°C. The kaolinite clay main characterization aspects were measured and are detailed as follow: (i) cation exchange capacity (CEC) = 6.74 mequiv./100 mg, (ii) surface area = 16.50 m^2g^{-1} and (iii) chemical oxides compositions: 44.31% SiO_2, 37.50% Al_2O_3, 2.30% CaO, 0.40% Fe_2O_3, 0.30% MgO, 0.08% K_2O and 0.03% Na_2O.

2.2.1. Preparation of glycine treated kaolinite clay

The natural Sinai Catharine clay was primarily acid activated by 2 N HNO_3 (clay/H^+ ratio = 1/1). The prepared suspension was refluxed for 48 h. The resulting activated clay was filtered and washed with distilled water several times to remove excess NO_3^{-1} ions and then, dried at 200°C under N_2 atmosphere for 4 h. The as-prepared kaolinite clay, nominated by NK, (100 g) was again refluxed in aqueous solution of glycine hydrochloride (182 mM/l) at pH~5.0 for 4 h. Thereafter, the mixture was filtered and the solid fractions were then washed several times by distilled water and acetone before being finally dried at 170°C for 18 h in dry air and abbreviated by GK kaolinite sample. The chosen concentration of glycine hydrochloride was

nearly threefold the CEC of natural kaolinite in order to ensure occupation of glycine species upon different kaolinite sites, viz., cation exchangeable sites, Brønsted acid sites, silanols, aluminols, and high adsorption potential surface and edge sites.

2.2.2. Preparation of diamino-modified glycine treated kaolinite

In three different batches, each will be subjected by a suspension of appropriate amount of glycine treated kaolinite clay in methanol and the clay/solvent ratio becomes = 1:6. For the first batch, ethylenediamine (0.7 ml) was dropped gently onto the suspension. The mixture was refluxed at 70°C for 72 h. The modified clay was separated by filtration, washed several times by distilled water and methanol, dried at 100°C for 24 h and then ground to fine powder being symbolized by AK1 kaolinite sample. The same procedure was followed in preparation of phenyl hydrazine and polyoxopropylenediamine modified glycine treated kaolinite, which are symbolized by AK2 and AK3 kaolinite, respectively. The amounts of phenyl hydrazine and polyoxopropylenediamine conducted in the second and third batches are 1.0 and 1.25 ml, respectively. The concentrations of diamino-modifiers were chosen to be almost one-third the CEC of natural kaolinite.

2.3. Characterization of clay adsorbents

The physicochemical characteristics of native and modified Sinai kaolinite clays were performed using the conventional techniques of: FTIR spectroscopy (using FTIR 4100 type A from JASCO company, USA, with resolution 2 cm^{-1}) and XRD spectrometer (with BRUKER D_8 ADVANCE, Germany operated at, 40 kV and 40 mA using Ni-filtered Cu Kα radiation $\lambda = 1.5418$ Å). The texture of the samples was investigated via BET surface area determination and pore size analysis, based on adsorption–desorption isotherms of N_2 at 77 K [22] after samples outgassing at 200°C for 4 h. The morphology features were studied and revealed using scanning electron microscope, (SEM, of model JEOL-JSM T2000, camera of model JEOL-T20-CSI).

The CEC was measured, in mequiv./100 g, using sodium acetate procedure (method 9081) [23].

The surface acid–base behaviors were followed up potentiometrically [24] adopting the suggested three-site model [25,26]. The site density of amphoteric aluminols (D_{AlOH}) was derived from the number of edge aluminol surface charges, $\sigma_{H(edge)}$, (at pH's, 5–8). The basal plane cation exchange site density (D_{CE}) was based on the number of basal proton surface charges, $\sigma_{H(basal)}$, estimated from CEC [26,27] (at pH ≈ 4). The site density of acidic silanols (D_{SiO^-}) was calculated from the number of edge silanol surface charges, $\sigma_{O^-(edge)}$ (at pH's > 8). The surface charge site densities, D_x, (sites nm^{-2}), could thus be determined according to the equation [27,28]; $D_x = \sigma_x$ (mmol L^{-1} g^{-1}) N_{Av}/S_{BET}, where, N_{Av} is Avogadro's number and S_{BET} (nm^2 g^{-1}) is the specific surface area of the sample. The Point of zero net proton charge (PZNPC) was also estimated [26].

2.4. Adsorption experiments

The batch adsorption experiments were carried out in 100 ml Erlenmeyer flasks by mixing the allocated clay suspension, containing 0.25 g kaolinite clay dispersed in 20 ml deionized water, with 30 ml aqueous solution of metal ions (Cu^{2+}, Ni^{2+} and Zn^{2+}). Thereafter agitate the mixture at 25°C for the desired time intervals. After achieving the required adsorption state, the mixture was centrifuged (Remi R 24, 20,000 rpm) and the metal ions, remaining unadsorbed in the supernatant liquid were determined with Atomic Absorption Spectroscopy (AA240FS, Varian, USA). Only two different conditions, including the contact time and initial adsorbate concentration, were tested. The pH and adsorption temperature were maintained, during the whole adsorption experiments, at pH ~ 5 and 30°C regarding to the needed environmental opportunities in severe contaminated water depollution processes, besides avoiding the development of colloidal metal hydroxides at higher pHs [9]. The pH during adsorption processes was maintained using either 0.01 N NH_4OH or 0.01 N HNO_3. The following conditions were intended for different sets of experiments:

2.4.1. Effects of adsorbate concentration

Cu(II): Clay 8 g/l, temperature 30°C, pH 5.7, time 120 min, Cu(II) concentration 25, 100, 400, 800, 1,500, 2,300, 4,000, 5,000, 8,000 mg/l,

Ni(II): Clay 8 g/l, temperature 30°C, pH 5.7, time 120 min, Ni(II) concentration 20, 100, 600, 900, 1,800, 3,800, 6,000, 8,000 mg/l,

Zn(II): Clay 8 g/l, temperature 30°C, pH 5.7, time 120 min, Zn(II) concentration 15, 100, 500, 1,000, 2000, 4,000, 6,000, 8,000 mg/l,

2.4.2. Effects of interacting time and adsorption kinetics

Cu(II): Clay 8 g/l, Cu(II) 800 mg/l, temperature 30°C, pH 5.7, time 0.5, 1.00, 1.50, 2.50, 5.00, 7.00, 10.00, 15.00, 20.00, 27.00 min,

Ni(II): Clay 8 g/l, Ni(II) 600 mg/l, temperature 30˚C, pH 5.7, time 0.25, 0.50, 1.25, 2.00, 3.00, 5.00, 6.50, 8.50, 11.00 min,

Zn(II): Clay 8 g/l, Zn(II) 500 mg/l, temperature 30˚C, pH 5.7, time 0.5, 0.50, 0.70, 1.00, 1.50, 2.50, 3.70, 5.60, 7.50, 9.00 min,

The amount, q, of metal ions adsorbed per unit mass of the adsorbent ($mg\,g^{-1}$) and the extent of adsorption (%) are computed from the expression, $q = (C_0 - C_t)/m$,

$$\% \text{ adsorption} = (C_0 - C_t) \times 100/C_0$$

where C_0 (mg/l) and C_t (mg/l) are metal ions concentrations before and after adsorption for time t, and m (g) is the amount of clay adsorbent taken for 1l of solution.

2.5. Theoretical foundation

The adsorption equilibrium is usually described by an isotherm equation whose parameters express the surface properties and affinity of adsorbent. The following two widely used isotherms [29,30] are usually applied:

(a) Linear form of Freundlich isotherm: $\log q_e = \log K_f + n \log C_e$

(b) Langmuir isotherm: $\frac{C_e}{q_e} = \frac{1}{bq_m} + (\frac{1}{q_m})\,C_e$

where C_e and q_e are the equilibrium concentration of metal ions in the liquid phase and in the solid phase, respectively. The Freundlich coefficients, K_f ($mg^{1-1/n}L^{1/n}g^{-1}$) and n, are related to adsorption capacity and adsorption intensity of the solid adsorbent, respectively. Similarly, b and q_m are Langmuir coefficients representing the equilibrium constant for the adsorbate–adsorbent equilibrium ($l\,g^{-1}$) and the monolayer capacity of the solid ($mg\,g^{-1}$), respectively.

The kinetics of the adsorption processes were studied using both pseudo-first-order [31–33] and second-order models [34–36] for the rate expression given, respectively, by

(a) $\ln (q_e - q_t) = \ln q_e - k_1\, t$

(b) $t/q_t = 1/(k_2\, q_e^2) + t/q_e$

where k_1, k_2, q_e and q_t represent the pseudo-first-order rate constant (min^{-1}), second-order rate constant ($g\,mg^{-1}\ min^{-1}$), adsorption capacity of the clay adsorbent ($mg\,g^{-1}$) and the amount of metal ions adsorbed at time t ($mg\,g^{-1}$), respectively.

For porous substrates, there are possibilities for diffusion of adsorbate species either from liquid bulk phase up to the adsorbent surface or within pore channels. In adsorption systems, where there is a possibility of intraparticle diffusion being the rate limiting step, the intraparticle diffusion approach described by Weber and Morris is used [37]. The rate

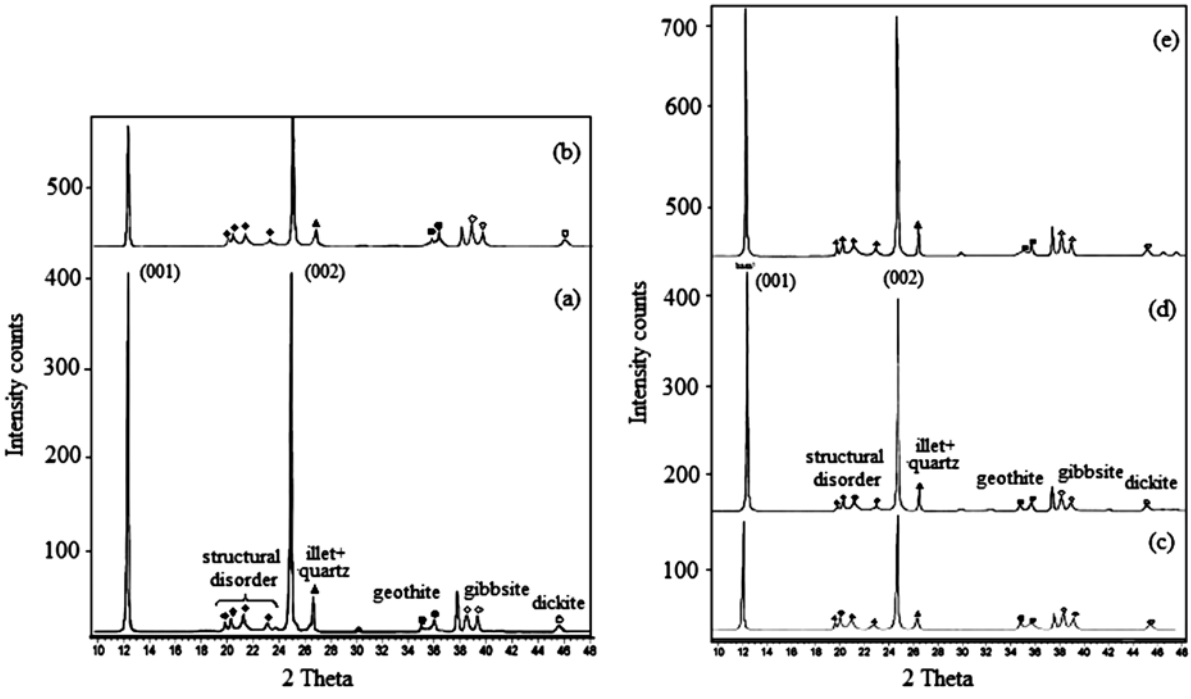

Fig. 1. XRD patterns of (a) natural kaolinite, (b) glycine treated kaolinite, and amino-modified glycine treated kaolinite through, (c) ethylenediamine, (d) phenyl hydrazine and (e) polyoxypropylenediamine.

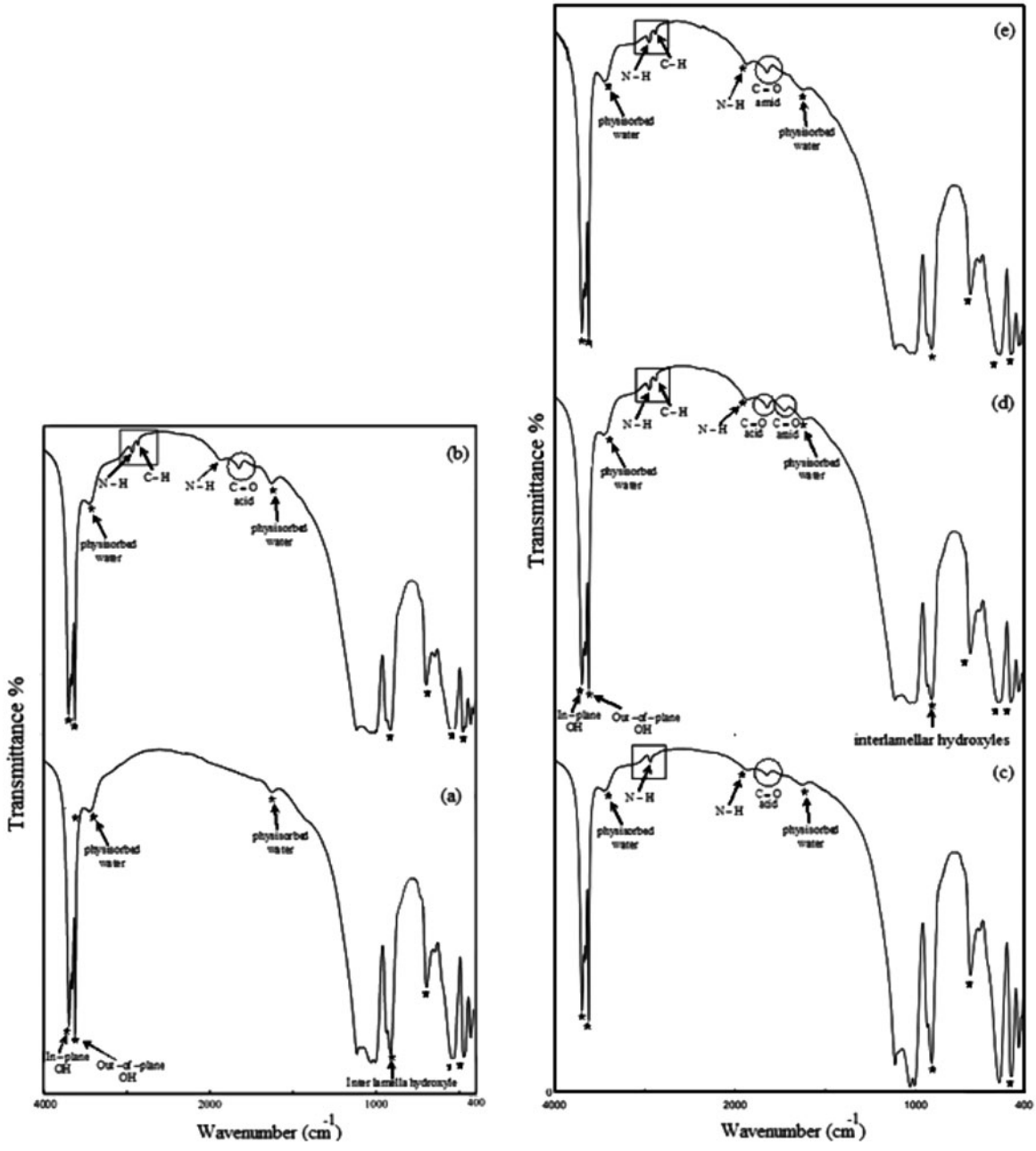

Fig. 2. FTIR spectra of (a) natural kaolinite, NK, (b) glycine treated kaolinite, GK, (c) ethylenediamine modified glycine treated kaolinite, AK1, (d) phenyl hydrazine modified kaolin/poly(glycine) composite, AK2 and (e) polyoxypropylenediamine modified kaolin/poly(glycine) composite AK3.

constants, for intraparticle diffusion (k_i) are determined using equation [31,38] given below:

$$q_t = k_i t^{0.5}$$

The k_i being the slope of straight line portions of plot q_t vs. $t^{0.5}$. These plots generally have dual nature, i.e. initial and final linear portions. The initial portions represent the boundary layer diffusion effects while the final portions are the result of intraparticle diffusion effects [39,40].

3. Results and discussion

3.1. XRD study

The XRD patterns of natural Sinai kaolinite and its derivatives are shown in Fig. 1. The XRD pattern of

Table 1
Chemical composition of Sinai natural kaolinite and various diamino-modified kaolin determined by XRF

Adsorbents	Chemical composition (%) by XRF							Si/Al
	SiO_2	Al_2O_3	Fe_2O_3	CaO	MgO	Na_2O	K_2O	
NK	44.31	37.45	0.41	2.28	0.29	0.03	0.08	1.18
GK	51.35	33.21	0.32	0.05	0.30	0.02	0.01	1.34
AK1	46.21	35.77	0.31	0.04	0.00	0.00	0.01	1.30
AK2	45.38	35.19	0.31	0.04	0.00	0.00	0.01	1.30
AK3	43.76	33.84	0.31	0.04	0.00	0.00	0.01	1.30

Table 2
Surface acid-base properties and cation exchange capacities of natural and various diamino-modified kaolinite samples

Adsorbents	CEC (meq/100 mg)	PZNPC	Surface charge site densities		
			D_{SiO^-}	D_{AlOH} (sites nm^{-2})	D_{CE}
NK	6.7	4.5	266	120	240
GK	9.9	3.3	924	46	98
AK1	5.1	3.9	345	117	210
AK2	3.6	3.6	386	19	41
AK3	4.9	3.8	2,381	456	1,098

the natural kaolinite generally shows a basal (0 0 1) and (0 0 2) reflections at $2\theta \sim 12.35^\circ$ and 24.90°, respectively assigning to the interlayer basal space [10]. The $k \neq 3n$ reflections [(0 2 0), (1 $\bar{1}$ 0), (1 1 $\bar{1}$) and (0 2 1)] at $2\theta = 19.87^\circ$, 20.4°, 21.2° and 23°, respectively, are characteristic of the structural disorder of interlamellar sheet structure [41]. The diffraction peaks corresponding to the admixture minerals in various kaolinite samples were observed at $2\theta = 26.62^\circ$, [34.99° and 35.96°], [38.45° and 39.28°] and 45.50°, which correspond to illite + quartz, goethite, gibbsite and dickite, respectively. It is clearly evident from the XRD patterns of different modified kaolinite samples that the crystallinity and interlamellar structure of kaolinite is intact with low considerable deformations. This implies that treatment of kaolinite via amino acids as well diamino compounds most probably led to either surface or edge modifications rather than intercalation.

3.2. Affirmation of chemical structure through FTIR study

FTIR spectra of natural kaolinite and its modified derivatives are depicted in Fig. 2. For natural

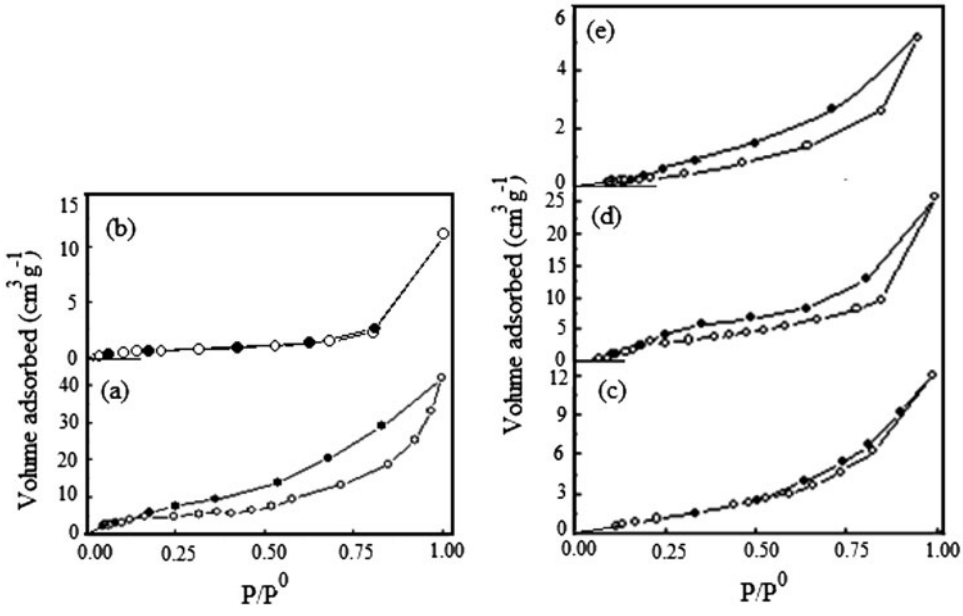

Fig. 3. Representative adsorption-desorption isotherm of N_2 at −196°C on: (a) NK, (b) GK, (c) AK1, (d) AK2 and (e) AK3.

kaolinite, the strong bands at 3,715 and 3,619 cm^{-1} correspond to the in-plane hydroxyls of the inner surface (inner inaccessible surface hydroxyls) and the out-of-plane hydroxyls of the inner surface (outer accessible surface hydroxyls), respectively [42]. The absorption bands at 3,500 and 1,600 cm^{-1} are related to the adsorbed water molecules within the clay interlayers or located onto the surface of silica tetrahedral sheet structure [43]. The strong absorption bands in the 1,000–1,200 cm^{-1} region reflect stretching vibrations of Si–O groups in the silicate structure, namely, asymmetric stretching vibrations of apical oxygen of SiO_2 tetrahedra [42]. The FTIR bands at 695, 548 and 476 cm^{-1} are assigned to Si–O–Al vibrations [43]. The band at 917 cm^{-1} is characteristic to the interlamellar Al–OH hydroxyl groups of kaolinite clay [42].

For FTIR spectrum of glycine treated kaolinite clay (GK, Fig. 2), the bands referred to the in-plane, out-of-plane hydroxyls of the inner surface and the interlamellar hydroxyls were marginally shifted lower. This displacement implies existence of considerable sort of interactions between glycine species and surface hydroxyls of the clay mineral. Also, bands characteristic for glycine molecules seem to appear at 2,978, 2,848 and 1,793 cm^{-1} corresponding to N–H, C–H and carboxylic C=O stretching vibrations, respectively.

Ethelyenediamine modifier did not affect the mutual interactions between glycine species and clay hydroxyls, whereas the bands characteristic for in-plane, out-plane and interlamellar hydroxyls appeared at stretching vibrations similar to that in glycine treated kaolinite. This may endorse existence of ethylenediamine species onto kaolinite clay surfaces in individual inactive manner.

FTIR spectrum of phenylhydrazine modified glycine treated kaolinite (AK2, Fig. 2) shows shifting in the bands characteristic for in-plane, out-of-plane hydroxyls of the inner surface and interlamellar hydroxyls indicating preferential interactions between

Table 3
Surface parameters of the various diamino-modified kaolinite under study

Adsorbents	S_{BET} ($m^2\ g^{-1}$)	$V_p^{0.95}$ (ml g^{-1})	$\bar{\rho}_h^{PP}$ (Å)	S_t ($m^2\ g^{-1}$)	$\bar{\rho}_h{}^{PP}{}_{most\ abund}$[a] (Å)
NK	16.47	0.0652	79.10	17.28	0.27–0.48
GK	4.30	0.0198	92.07	4.62	0.18–0.38
AK1	6.87	0.0186	54.23	6.69	1.72
AK2	10.31	0.0400	77.61	11.23	0.47–0.85
AK3	1.07	0.0080	19.01	1.28	0.45–0.92

Note: [a]Calculated from PSD.

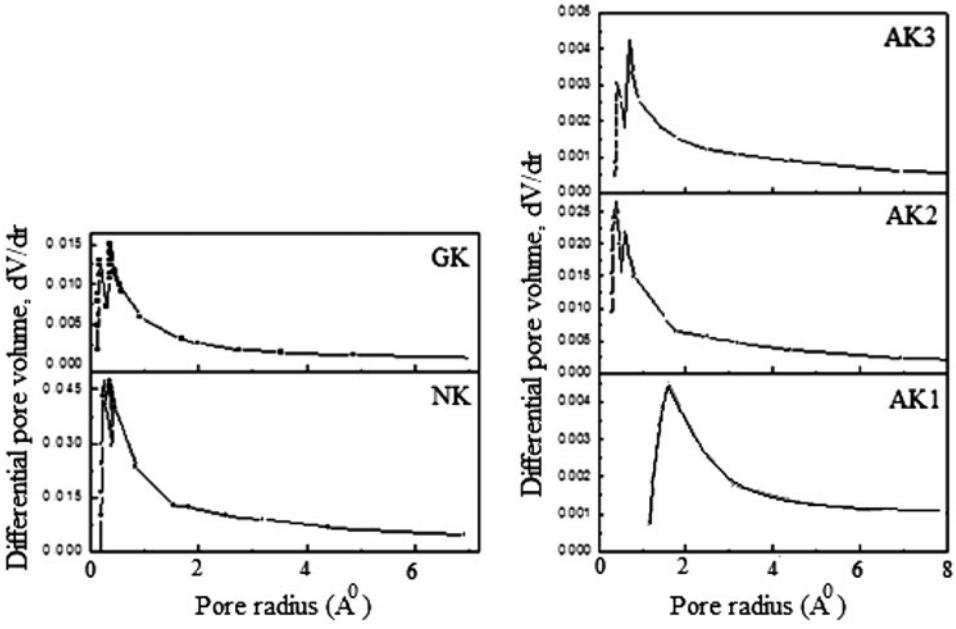

Fig. 4. PSD curves for (a) NK, (b) GK, (c) AK1, (d) AK2 and (e) AK3.

phenyl hydrazine and glycine molecules at the expense of interaction occurred between glycine molecules and surface hydroxyl groups. Interestingly, phenyl hydrazine modifier speculates to vehicle step polymerization of glycine molecules over kaolinite clay surfaces founding kaolin/poly(glycine) composites. This is clearly evident by appearance of new band at 1,750 cm^{-1} assigned to C=O stretching frequencies characteristic for amide groups. However, a band at 1,795 cm^{-1} assigned to C=O of −COOH group, is still acted pointing to existence of some unpolymerized glycine molecules, being most probably tightly packed with the inner surface hydroxyls far away from the effective polymerization field of phenyl hydrazine.

FTIR spectrum of polyoxypropylenediamine modified glycine treated kaolinite reveals vanishing of the band referred to C=O characteristic for carboxylic groups besides attendance of a peak at 1,760 cm^{-1} characteristic for C=O of amide groups. This manifests the strong interaction between glycine and the long-chain alkyl diamine molecules, which thereby allow step polymerization of glycine molecules within kaolinite interlamellar spacing originating large polypeptide chains onto kaolinite surface developing kaolin/poly(glycine) composite. The bands assigned to in-plane and out-of-plane hydroxyls of the inner surface and interlamellar hydroxyls are slightly shifted, being lower than that appeared in the spectrum of natural kaolinite and higher than that observed in GK clay sample. This may reveal the favoured conjugation of polyoxypropylenediamine with various kaolinite surface hydroxyls.

3.3. Chemical constituent's analysis

The results derived from chemical analysis by XRF (Table 1) reveal that treating kaolinite via glycine

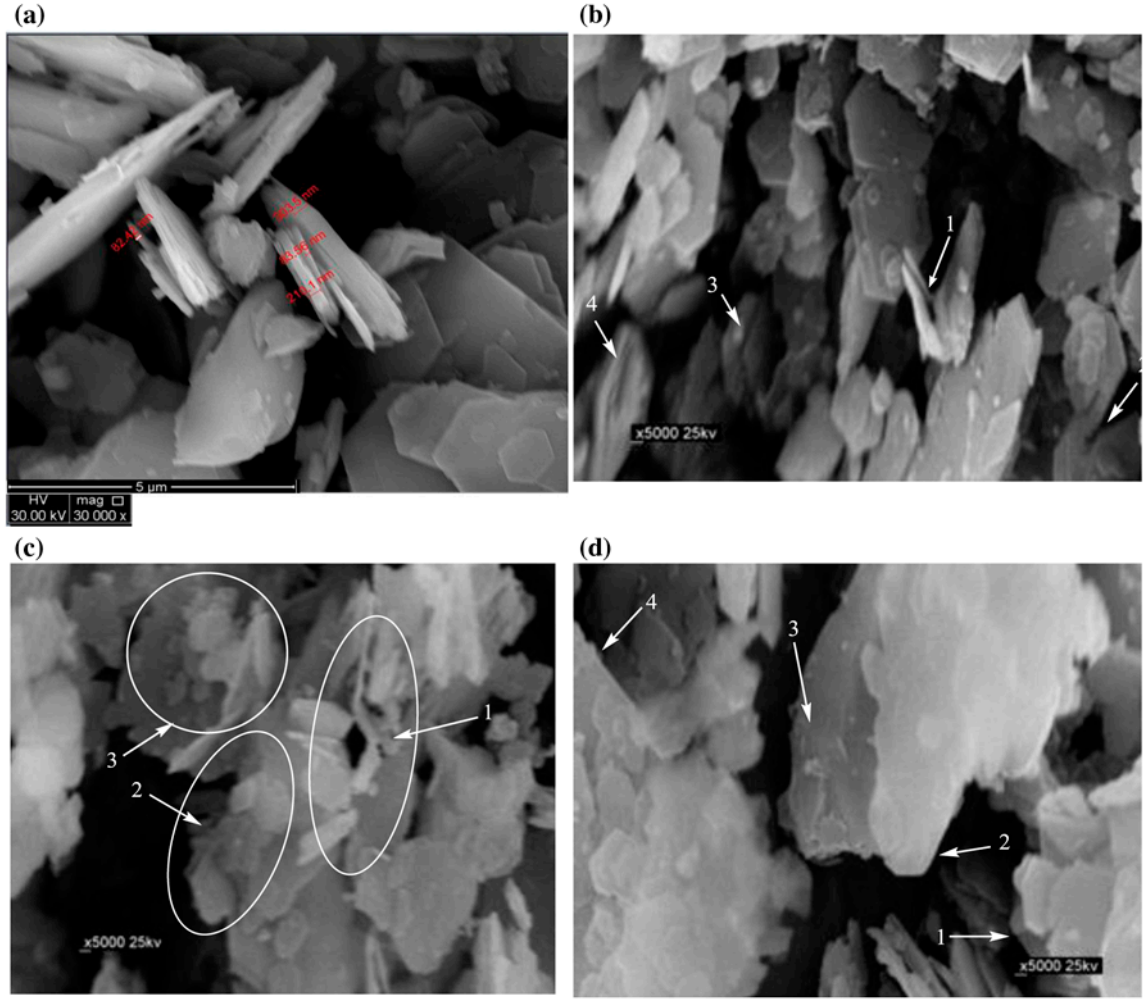

Fig. 5. Scanning electron micrographs of Sinai natural kaolinite (a), glycine treated kaolinite (b), ethylenediamine modified glycine treated kaolinite (c) and polyoxopropylenediamine modified kaolin/poly(glycine) composite (d).

species led to considerable increase in both the percentage of tetrahedral SiO_2 sheet (from 44.31 to 51.35%) and the Si/Al ratio (from 1.18 to 1.34). Such increment could be related to the dealumination of octahedral sheets with noticeable leaching of exchangeable cations (cf., Fe^{3+}, Ca^{2+}, Mg^{2+} and K^{+}) resulting in more protruding for tetrahedral SiO_2 sheet structure. Modification of glycine treated kaolinite sample via different diamino- compounds causes slight depression in Si/Al ratio (1.34–1.30), complete reduction of Mg^{2+} exchangeable cation, located mostly in the octahedral sheet structure bonded to Al, and decreasing in SiO_2% indicate successful insertion of various diamino-modifiers within the kaolinite interlamellar spaces allowing thereby its interaction with various clay sites (viz., SiO_2 tetrahedral structure, Al octahedral structure and, edged and interlayered exchangeable cations).

3.4. Acid–base characteristics and cation exchange capacities

Changes in the surface acid–base properties of modified kaolinite were followed up potentiometrically [24], applying the recently reported three-site model [25,26]. CEC, determined according to [23], PZNPC [26] and calculated surface charge densities for the studied kaolinite samples are included in Table 2.

It is evident from Table 2 that, the natural kaolinite exhibits a quite low CEC characterizing Tetrahedral/Octahedral sheet (TO) structure in agreement with the reported values [7]. For glycine treated kaolinite, the increase in CEC (which represents the actual exchangeable sites) and the loss of about half the original basal CE-site density (D_{CE}, represents the overall sites capable for cation exchange) may be correlated to such interactions between glycine species and Al octahedral

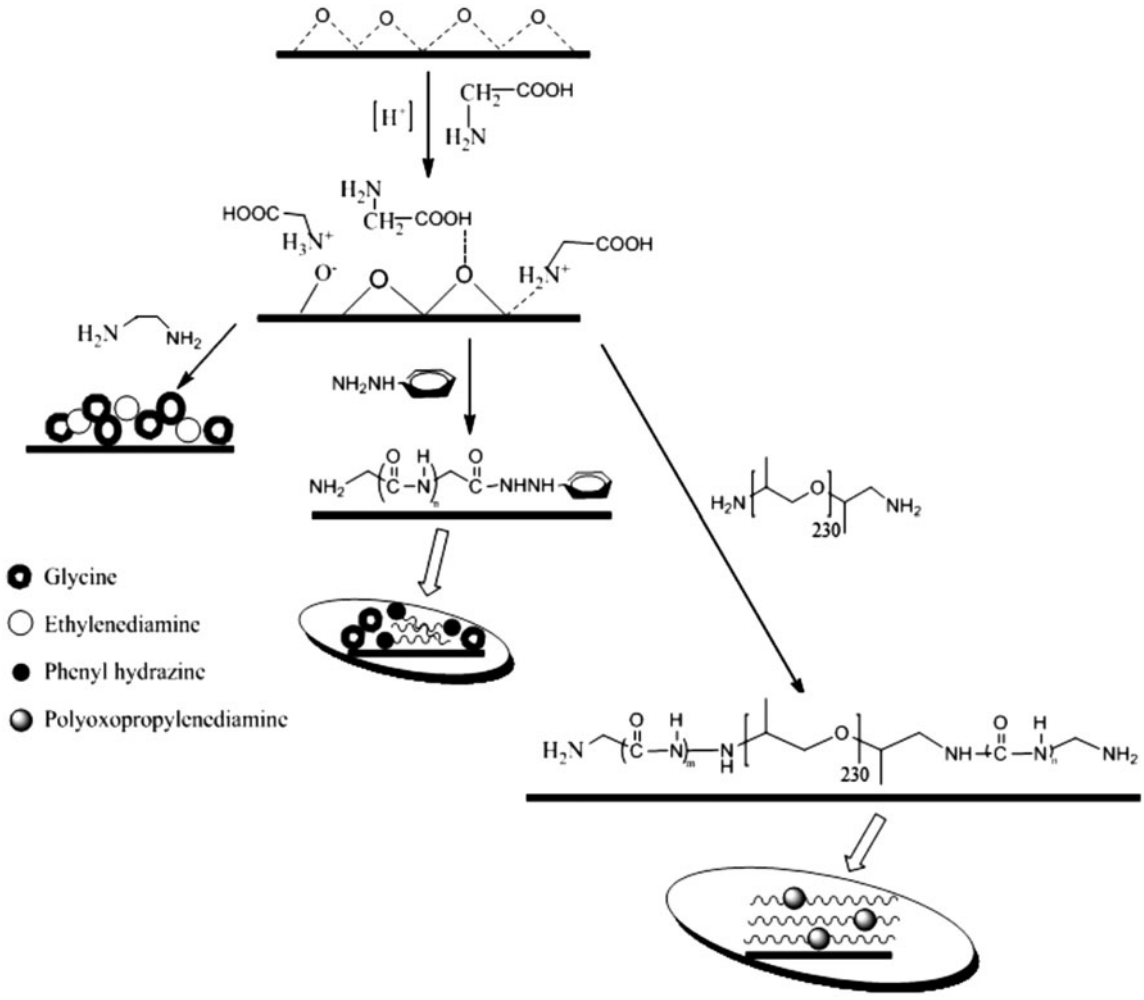

Scheme 1. Schematic diagram of *in situ* glycine polymerization acts within kaolinite clay sheets to evaluate diamino-modified kaolin/poly(glycine) composites.

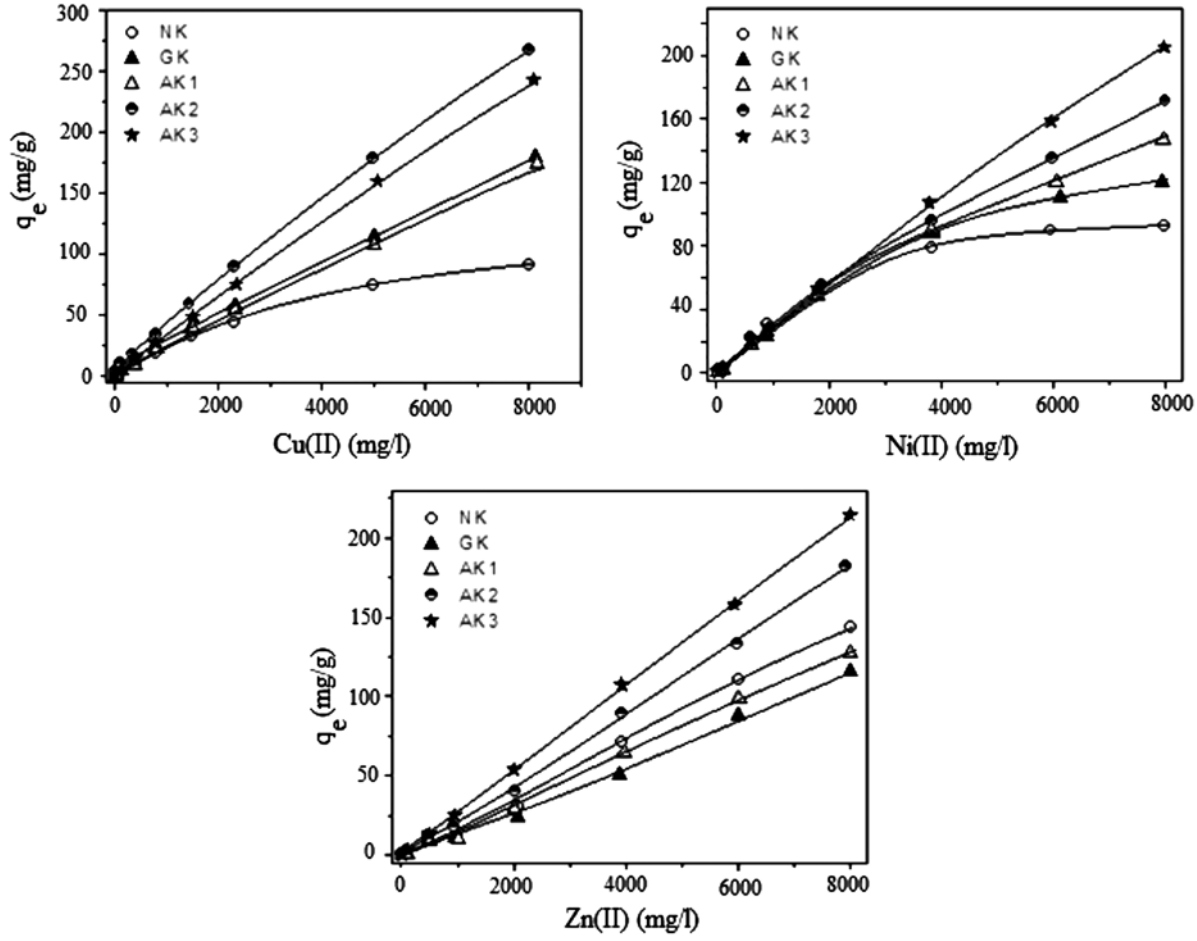

Fig. 6. Amount of metal ions adsorbed per unit mass (q_e) onto various diamino-modified kaolin samples as a function of initial metal concentration at 30°C (clay 8 g/l, pH 5.7, time 120 min).

sheet structure resulting in mask fewer of foreign cations like Mg^{2+}, Ca^{2+} and Fe^{3+} from being exchanged. The progressive increase in D_{SiO^-} along with the marked decrease in D_{AlOH} confirm the role of glycine species in breaking the tetrahedral Si–O–Si bridges and reforming the octahedral Al–O–Al bridges. In this respect, the PZNPC shows a significant decrease points to generation of newer acid sites.

By modification of glycine treated kaolinite clay via different diamino- compounds, the acid–base behaviours seem to be strongly affected, in terms of the decrease in CEC and the great changes in surface site densities, as compared with GK sample, while the PZNPC is nearly unchanged (~3.7) (Table 2). The diminish in CEC values, are interrelated to the screening effect of different amino-species toward some of the exchangeable cations that are deeply located in the interlayer space [9], whereas the PZNPC corresponds to the modified kaolinite samples (~3.7, Table 2) are relatively higher than that corresponds to glycine treated kaolinite referring most probable to the basic character of -NH_2 group together with peptide linkage (–CO–NH–). Ethylenediamine modifier leads selectively to regaining Si–O–Si causing a marked decrease in silanols site density, D_{SiO^-}. Similarly, modification of GK by phenyl hydrazine declines surface charge densities (D_{SiO^-}, D_{AlOH}, D_{CE}) being perhaps linked to the ability of phenyl hydrazine species to reinstate Si–O–Si, Si–O–Al and Al–O–Al bridges. The reformed silica as well alumina bridges may impede the interlayer foreign cations, viz., Na^+, $Fe^{3+}$and Ca^{2+} from being exchanged resulting in significant decrease in D_{CE}. For AK3 sample, the large fractions of polypeptides, being formed from catalytic step polymerization of glycine species, as previously evidenced from FTIR studies, display the prominent role in the breakage of Si–O–Si, Si–O–Al and Al–O–Al producing plenty of silanols, aluminols and much more interlayer cation exchange sites (cf., marked increase in D_{SiO^-}, D_{AlOH} and D_{CE}).

3.5. Textural and morphological investigation of native and modified kaolinite samples

The obtained adsorption–desorption isotherms of N_2 at −196°C on the surface of natural and modified kaolinite samples are illustrated in Fig. 3, being almost of type II in the classification of Sing et al. [22]. The closed hysteresis loops in the case of natural kaolinite and its modified derivatives particularly, amino-modified glycine treated kaolinite are of type H3, which characterizes mainly mesoporous solid, often associated with agglomerates of plate-like particles containing slit-shaped pores [22]. For GK treated kaolinite, the completely reversible isotherm may be linked with evolution of larger fraction of mesopores.

The derived surface parameters are given in Table 3 including specific surface areas (S_{BET}, $m^2 g^{-1}$), pore volumes (V_p, $ml\,g^{-1}$) estimated at 0.95 P/P^o, and average pore radii ($\bar{\rho}h^{PP}$) and most abundant pore radii ($\bar{\rho}h^{PP}_{most\,abund}$), which derives from pore size distribution (PSD) curves) assuming parallel plate pore model. The surface parameters characterizes natural kaolinite are in agreement with those reported in the literature [44]. The specific surface area and the total pore volume of GK are significantly lower than that of NK reflecting the deformation of octahedral sheet structure through leaching of some exchangeable cations. The glycine species seems to populate beneath the edges of kaolinite interlayers as proved by elevation of the average pore radii, which represents pore mouth dimensions, linked with depression in the most abundant pore radii, which denotes dimensions of the middle part of pores. Such orientation may be a reasonable issue for pore blockage and sharp decrease in the specific surface area (16.5–4.3 $m^2 g^{-1}$).

For AK1 modified kaolinite, declining in surface parameters (S_{BET}, V_p and $\bar{\rho}_h{}^{PP}$) together with the boosting in $\bar{\rho}_h{}^{PP}{}_{most\ abund}$ are most probably related to the function of ethylenediamine modifier in driving glycine molecules deeply inside the pores adopting large fractions of pores having wider dimensions in its middle part linked with narrower extents at the neck. The surface properties of phenyl hydrazine modified kaolinite are returned to be nearly similar to that of natural kaolinite (from 16.5 to 10.3 $m^2 g^{-1}$, Table 3). Such textural analogue together with the appearance of micropores of most abundant pore radius of ~0.85 Å could be attributed to the mutual coexistence of various features of glycine oligomers in addition to smaller fractions of unpolymerized glycine species either beyond pore mouth and/or deeply intercalated within the interlamellar pore space. For polyoxypropylenediamine kaolin/poly(glycine) composite, the progressive lowering in specific surface area (S_{BET}), total pore volume (V_p) and average pore radii ($_h{}^{PP}$) are strongly correlated to the large polypeptide chains formed in kaolinite interlayers. These *in situ* poly(glycine) species lead to severe pore collapse due to the probable hydrogen bonds originated between the TO interlamellar sheet structure, by its silanols and aluminols, and the peptide linkage (–CO–NH–) of polymeric chains.

For supplementary pore structural revelation, V_l−t plots were constructed from the adsorption data, where, V_l is the volume of N_2 ($ml\,g^{-1}$) and t is the statistical thickness in Å, which derives from the reference t-curves [45]. The surface areas (S_t, $m^2 g^{-1}$) estimated from the V_l−t plots are in good conformity with S_{BET} values (Table 3) ensuring the correct choice of the reference t-curves. The obtained V_l−t plots revealed the prevalence of mesopore fractions in the natural and modified kaolinite samples, as evidenced by the average pore radii values ($\bar{\rho}_h{}^{Pp} > 10$ Å).

For further investigation of the existing pore systems, PSD curves of various kaolinite samples are depicted in Fig. 4. It is obvious that, the bimodal pore

Table 4
Freundlich and Langmuir coefficients for adsorption of metal ions at 30°C (clay 8 g/l; initial metal ion concentrations for Cu(II): 25, 100, 400, 800, 1,500, 2,300, 4,000, 5,000, 8,000 mg/l, Ni(II): 20, 100, 600, 900, 1,800, 3,800, 6,000, 8,000 mg/l, and Zn(II): 15, 100, 500, 1,000, 2000, 4,000, 6,000, 8,000 mg/l; pH 5.7; time 120 min)

Metal ions	Clay	Freundlich coefficient			Langmuir coefficients
		K_f ($mg^{1-1/n} L^{1/n} g^{-1}$)	n	r^2	r^2
Cu(II)	NK	0.012	1.06	0.93	−0.15
	GK	0.058	0.92	0.99	0.83*
	AK1	0.016	1.07	0.98	−0.13
	AK2	0.432	0.73	0.98	0.52
	AK3	0.153	0.84	0.99	0.46
Ni(II)	NK	0.018	1.03	0.80	−0.90
	GK	0.030	0.98	0.95	0.14
	AK1	0.024	1.02	0.97	−0.09
	AK2	0.057	0.93	0.98	0.62
	AK3	0.080	0.90	0.99	0.79**
Zn(II)	NK	0.002	1.27	0.97	0.08
	GK	0.024	0.94	0.97	−0.18
	AK1	0.002	1.25	0.97	0.17
	AK2	0.044	0.93	0.98	−0.19
	AK3	0.131	0.83	0.97	0.03

Note: *Apply Langmuir model; $b = 0.069\,l\,g^{-1}$ and $q_m = 555.6\,mg\,g^{-1}$.
**Apply Langmuir model; $b = 0.075\,l\,g^{-1}$ and $q_m = 621.0\,mg\,g^{-1}$.

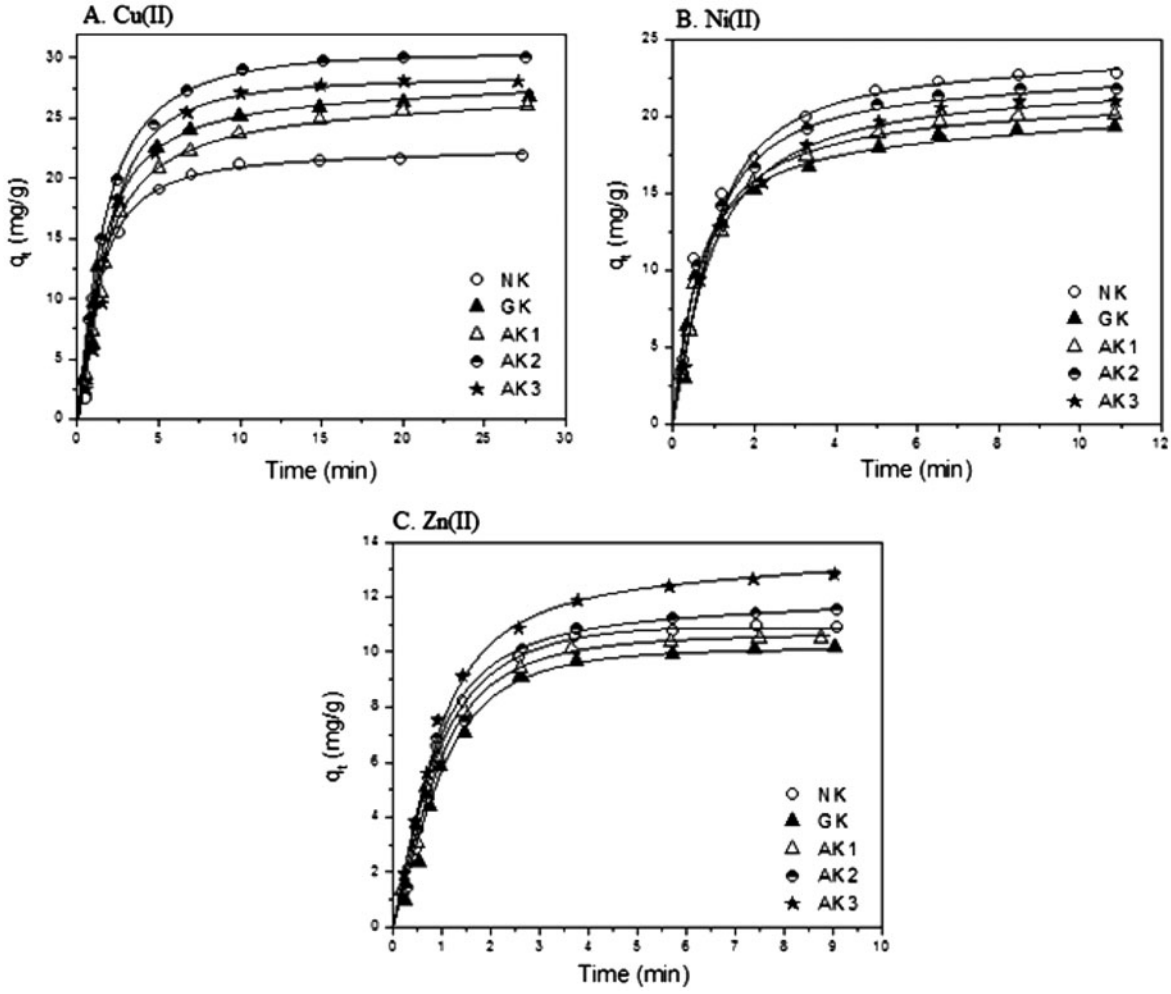

Fig. 7. Kinetic adsorption data for Cu(II) (A), Ni(II) (B) and Zn(II) (C) onto natural and various diamino-modified kaolin at 30°C (clay 8 g/l; pH 5.7; initial Cu(II): 800 mg/l; initial Ni(II): 600 mg/l; initial Zn(II): 500 mg/l).

system characteristic for natural kaolinite and glycine treated kaolinite is well-preserved during modification through phenyl hydrazine and polyoxypropylenediamine molecules. Kaolinite modification using ethylenediamine molecules was observed to eliminate wider PSD curve of larger fractions of most abundant pore radius $\sim$ 1.72 Å. In case of phenyl hydrazine and polyoxypropylenediamine modified kaolin/poly(glycine) composites, the PSD curves represent narrower bands of larger fractions of most abundant pore radii of 0.85 and 0.92 Å, compared to natural kaolinite, respectively. This phenomenon reflects the great dependence of $\bar{\rho}_h^{PP}{}_{\text{most abund}}$ onto the polypeptide fragments generated intensely in pore channels.

For more confirmation, SEM micrographs of modified kaolinite derivatives, namely; GK, AK1 and AK3, are compared with natural kaolinite in Fig. 5. The crystalline layered structure of the natural kaolinite is clearly evident in micrograph (a) showing regular and directed micro-sized flakes (from 80 to 300 nm). As seen in micrograph (b) for glycine treated kaolinite (GK), irregular and looser curved flakes were observed indicating structural deformation and disorder stacking of kaolinite clay layers, due to dealumination and accumulation of glycine species mostly beyond kaolinite edges as represented from elements 1, 2 and 3. In micrograph (c) for ethylenediamine modified glycine treated kaolinite (AK1), the clay flakes suffer much more fracture leads to smaller clay crystalline structure linked with carved edges (cf. zones 1,2,3). The polyoxypropylenediamine modified kaolin/poly(glycine) composite appears in micrograph (d) (AK3) was completely different from natural and other modified kaolinites. The *in situ* fashioned polypeptide chains, as evidenced from FTIR analysis, appear to be a main reason for manipulating a long range ordered and well-dimensioned kaolinite sheet structure. Hence, those *in situ* polymeric glycine

Table 5
Pseudo first and second order kinetics and intra-particle diffusion model parameters for the adsorption systems under study at 30°C (clay 8 g/l; pH 5.7; initial Cu(II): 800 mg/l; initial Ni(II): 600 mg/l; initial Zn(II): 500 mg/l)

Metal ions	Clay	Pseudo first-order model		Second-order model		Intraparticle diffusion			
		$k_1 \times 10^2$ (min^{-1})	r^2	$k_2 \times 10^2$ ($g\,in^{-1}$)	r^2	k_I^i ($mg\,g^{-1}min^{-0.5}$)	r^2	k_I^f ($mg\,g^{-1}min^{-0.5}$)	r^2
Cu(II)	NK	13.6	0.98	1.6	0.95	33.7	0.98	1.5	0.99
	GK	8.6	0.92	1.3	0.98	22.7	0.98	2.2	0.99
	AK1	9.0	0.97	1.3	0.99	16.4	0.99	2.4	0.99
	AK2	10.4	0.95	1.1	0.97	25.7	0.97	1.9	0.99
	AK3	10.8	0.95	0.7	0.95	20.6	0.99	2.0	0.99
Ni(II)	NK	27.3	0.97	4.4	0.99	28.9	0.99	2.6	0.99
	GK	19.2	0.98	5.5	0.99	34.3	0.99	2.0	0.98
	AK1	26.0	0.98	4.6	0.99	16.2	0.97	2.6	0.99
	AK2	32.5	0.93	5.5	0.99	15.5	0.98	2.4	0.99
	AK3	24.1	0.98	3.5	0.99	19.8	0.99	2.7	0.99
Zn(II)	NK	39.6	0.83	7.6	0.97	9.4	0.96	0.6	0.98
	GK	15.8	0.88	5.6	0.97	8.3	0.98	0.7	0.99
	AK1	42.7	0.83	7.9	0.97	8.5	0.98	0.6	0.98
	AK2	40.0	0.89	5.2	0.98	11.2	0.97	0.8	0.98
	AK3	38.8	0.81	6.9	0.97	10.0	0.99	1.0	0.99

species could be nominated as super binders, which induce clay sheet collapsing and heal the ruptured kaolinite platelets forming thereby fixed solids of well-defined matrices as shown in elements 1–4.

Based on the previous results of the physicochemical characteristics of natural kaolinite and its modified derivatives, a proposed schematic diagram expressing the in-function of amino-modifiers onto kaolinite interlamellar spaces was illustrated in Scheme 1.

3.6. Adsorption of Cu(II), Ni(II) and Zn(II) by modified kaolinite samples

All the adsorption experiments were done in triplicate under same conditions. The concentrations of the adsorbate in aqueous phase and in the solid phase were computed from the averages of experimentally determined metal ion concentration in the aqueous phase after adsorption. These values were then used in all subsequent treatment and analysis of data.

3.6.1. Effect of adsorbate concentrations

Amount of metal ions adsorbed per unit mass of variant kaolinite samples increased gradually with elevation of metal ions concentrations in the adsorbate solution (Fig. 6).

At low metal ion loading of less than 2,000 mg/l, the ratio of the number of metal ions to the number of available adsorption sites is considered small and consequently, adsorption will be largely dependent on the nature of adsorbate instead of the initial metal ion concentrations. The adsorption capacities for copper, nickel and zinc ions over various kaolinite fractions are closely similar indicating pronounced contribution of conventional kaolinite sites, e.g. silanols, aluminols and cation exchange sites, in various adsorption profiles rather than the modified kaolinite sites enchased by carboxylic groups, amino-species and poly peptide linkages. Interestingly, as the concentration of metal ions increased further than 2,000 mg/l, the nature of modified adsorption sites [46,47] as well the revelation ability for hidden adsorption zones become the crucial factor. Accordingly, phenyl hydrazine and polyoxypropylenediamine modified kaolin/poly(glycine) composites are then considered as the most suitable adsorbents for removal of Cu(II), Ni(II) and Zn(II) ions. By increasing the metal ion concentrations, the organized kaolinite layers most probably expand allowing adsorption of different metal ions upon the secreted adsorption sites, being located deeply inside the clay interlamellar spaces.

The empirical Freundlich coeffecients, n (0.83–1.27), the adsorption capacities, K_f (0.002–0.432 $mg^{1-1/n}$

$L^{1/n}\,g^{-1}$) and Freundlich correlation coefficients ($r^2 \sim 0.8$–0.99) for the uptake of Cu(II), Ni(II) and Zn(II) ions by natural and various modified kaolinite are depicted in Table 4. In most adsorption processes, the n values are nearly close to unity indicating seemingly that adsorption was favorable [48,49] and the adsorption sites were fully occupied, although the surface adsorption capacities exhibit much lower values. Such results are in conformity with the lower surface areas, S_{BET}, (1.0–16.0 $m^2\,g^{-1}$) and the lower most abundant pore radius, $\bar{\rho}_h^{PP}$, (0.18–1.72 Å). The results derived from Freundlich equation are closely congruent with Jiang et al. [48], who studied adsorption of Cu (II) and Ni(II) onto natural kaolinite clay and reported Freundlich adsorption capacity, K_f, of 0.14 and 0.095 $mg^{1-1/n}\,L^{1/n}\,g^{-1}$, respectively, while Zn(II) adsorption onto kaolinite is not seriously attempted yet.

Langmuir isotherm for adsorption of Cu(II), Ni(II) and Zn(II) ions onto natural and various modified kaolinite are also studied and their correlation coefficients (r^2) are illustrated in Table 4. Such coefficients are almost < 0.75, except for Cu(II) adsorption onto glycine treated kaolinite ($r^2 = 0.83$) and Ni(II) uptake onto polyoxypropylenediamine modified kaolin/poly(glycine) composite ($r^2 = 0.79$). However Langmuir coefficients for Cu(II) and Ni(II) uptake onto GK and AK3, respectively, are in agreement with Yavuz et al. [50], Langmuir capacities are significantly high. The elevated Langmuir capacities set kaolinite clay in competition with the most efficient adsorbents like carbon fiber [51], blast furnace [52] and Spirogyra species [53]. Thus, it is worth mentioning that the adsorption sites onto kaolinite clay were mostly non-uniform and nonspecific in nature being accord to the presence of various sites of altered potentials, i.e. silanols, aluminols, ion exchangeable sites, carboxylic amino- and peptide groups. Since Langmuir isotherm are applied in adsorption processes including probable chemical interactions between adsorbent and adsorbate, it is noticeable to regard the adsorption of Cu(II) and Ni(II) onto GK and AK3, respectively to the proposed chemical bonds originated between both Cu(II) and glycine carboxylic groups in GK sample, and Ni(II) and peptide groups in AK3 kaolin/poly(glycine) composite.

3.6.2. Effect of interacting time and kinetics of adsorption

Adsorption kinetic studies are the key to evaluating the effectiveness of an adsorbent. An evaluation of the amount of adsorbed molecules (q_t) as a function of adsorption time is presented in Fig. 7. The metal ions seem to interact rapidly with various accommodated kaolinite sites within the first three minutes. Afterwards, interactions slowed down and approached equilibrium in the previous five min. Phenyl hydrazine kaolin/poly(glycine) composite declares the best uptake for Cu(II) while natural kaolinite preserve the highest Ni(II) amount adsorbed. Polyoxypropylenediamine modified kaolin/poly(glycine) composite shows maximum adsorption for Zn(II) metal ion.

Attainment of equilibrium is influenced by several factors including the nature of adsorbent and adsorbate, and the mode of interactions between them. Surprisingly, the accelerative achievement of the adsorption equilibrium state has never been reported yet in literature ensuring thereby the unique crystalline assemble of Sinai kaolinite clay and its modified derivatives. Accordingly, it is imperative to study the adsorption kinetics in its early stage, where the high initial uptake rates may be attributed to the amplitude of various reinforced adsorption implemented sites.

Table 5 shows the rate constants k_1 and k_2 derived from pseudo-first-order and second-order models, respectively. The linear correlation coefficients of pseudo-first and second-order reactions are also demonstrated in Table 5.

The pseudo-first-order plots indicate good linearity ($r^2 \sim 0.85$ for Cu(II), $r^2 \sim 0.97$ for Ni(II), and $r^2 \sim 0.85$ for Zn(II)) and yielded the first-order rate constant in the ranges of 8.6×10^{-2}–13.6×10^{-2} min^{-1} for Cu(II) uptake, 19.2×10^{-2}–32.5×10^{-2} min^{-1} for Ni(II) uptake and 15.8×10^{-2}–42.7×10^{-2} min^{-1} for Zn(II) uptake with respect to the natural kaolinite and the four modified ones. On the other hand, second-order plots had a very good linearity ($r^2 \sim 0.97$ for Cu(II), $r^2 \sim 0.99$ for Ni(II) and $r^2 \sim 0.97$ for Zn(II)) and provided the second-order rate constant in the ranges of 0.7×10^{-2}–$1.6 \times 10^{-2}\,g\,mg^{-1}\,min^{-1}$ for Cu(II) uptake, 3.5×10^{-2}–$5.5 \times 10^{-2}\,g\,mg^{-1}\,min^{-1}$ for Ni(II) uptake and 5.2×10^{-2}–$7.9 \times 10^{-2}\,g\,mg^{-1}\,min^{-1}$ for Zn(II) uptake regarding to the natural and the four modified kaolinite clay. This emphasizes the actuality of dual adsorption model, which, in earlier interacted time, based on first-order mechanism. Such mechanism was very rapid, characterized by much higher rate constants, and the adsorption reaction becomes, mainly film-diffusion controlled disregarding metal ion concentration effect [54,55]. For entire sorption period, adsorption could be changed to follow second-order model considering clay–metal ion interactions and chemisorption possibilities [7,46]. Pseudo-first-order as well second-order rate constants are found in the order of Cu(II) <Ni(II)<Zn(II) for both natural kaolinite and various kaolinite derivatives. The Cu(II), Ni(II) and Zn(II) adsorption were quite prominent onto NK ($13.6 \times 10^2\,min^{-1}$, 1.6×10^2 $g\,mg^{-1}\,min^{-1}$), AK2

($32.5 \times 10^2\,min^{-1}$, $5.5 \times 10^2\,g\,mg^{-1}\,min^{-1}$) and AK1 ($42.7 \times 10^2\,min^{-1}$, $7.9 \times 10^2\,g\,mg^{-1}\,min^{-1}$), respectively. In turn, the preferential adsorption situations for Cu (II), Ni(II) and Zn(II) metal ions seem to be strongly correlated to the maximal ion exchange availability of natural kaolinite, the newly generated peptide groups in phenyl hydrazine modified kaolin/poly(glycine) composite, and the pronounced accretion of amino groups in ethylenediamine modified kaolinite, respectively.

The immense adsorption efficacy of kaolin/poly(glycine) composites, as illustrated in Fig. 6, cannot be only explained by the kinetics of the first- and second-order profiles but also studied through the kinetics of metal ions diffusion from solid–liquid interfaces to the interior of the kaolin/poly(glycine) composite. Therefore, the plots of q_t vs. $t^{1/2}$ according to intraparticle diffusion kinetics were debated (Fig. 8). The rate constant of initial external mass transfer (k_I^i), the rate constant of pore diffusion and chemisorption (k_I^f), and r^2 values were estimated from the slopes of the initial and final linear portions, being demonstrated by zone a&b, respectively, at various contact times (Fig. 8, Table 5). The results reveal that the diffusion rates decrease upon increasing the contact time. As the metal ions achieve the solid sorption field, the ionic species are attracted promptly toward the stronger external adsorption sites resulting in boundary layer diffusion effects, which are described by k_I^i. When most of the exterior adsorption sites are occupied, the unabsorbed metal ions are forced to diffuse into kaolinite micropores, where the pore diffusion rate constants could be detected from k_I^f. Both phenyl hydrazine and polyoxypropylenediamine modified kaolin/poly(glycine) composites exhibit the highest pore diffusion rate constant for Cu(II) ($1.9\,mg\,g^{-1}min^{-0.5}$ for AK2 and $2.0\,mg\,g^{-1}min^{-0.5}$ for AK3), Ni(II) ($2.4\,mg\,g^{-1}$

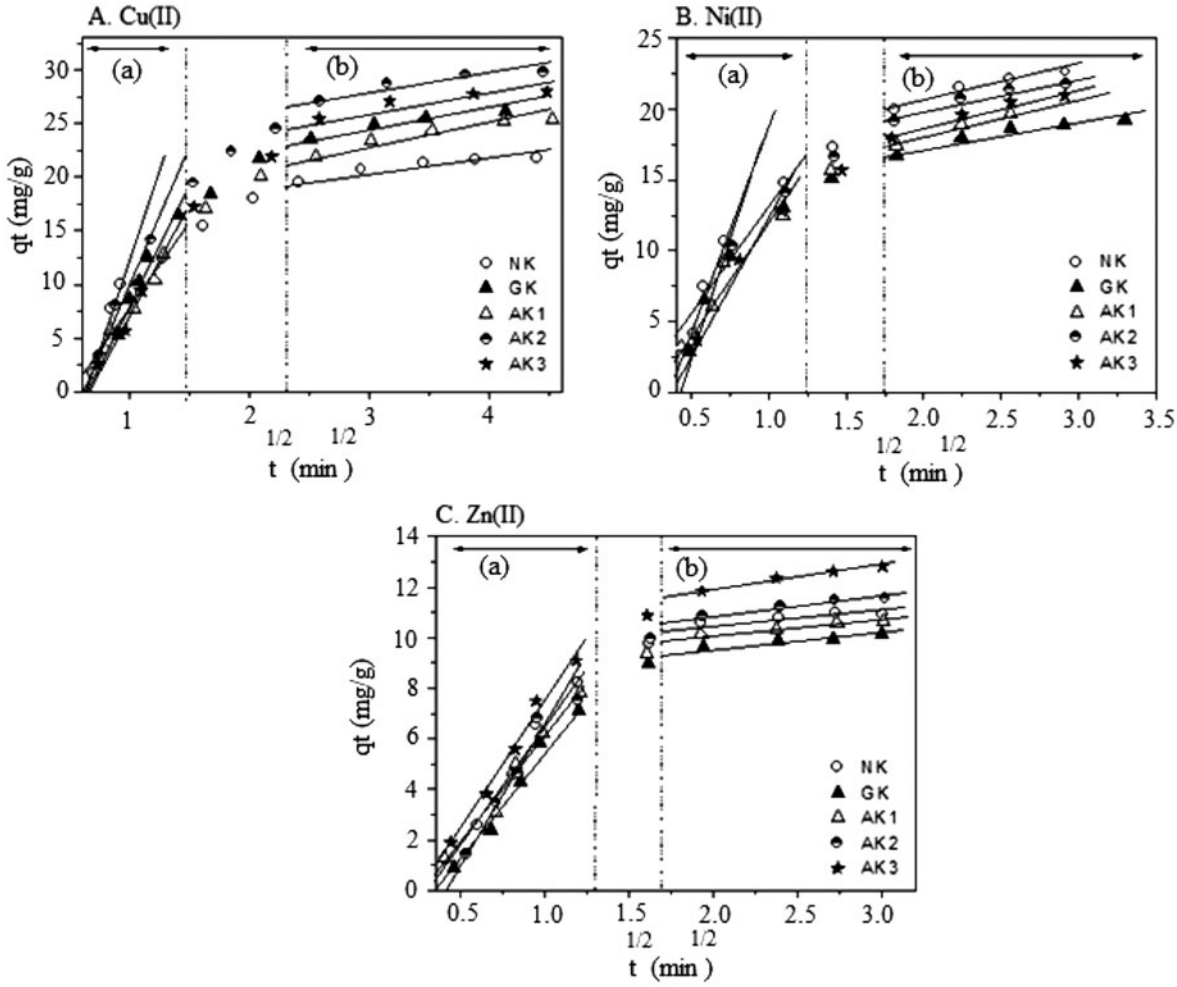

Fig. 8. Intra-particle diffusion model for the adsorption of Cu(II) (A), Ni(II) (B) and Zn(II) (C) onto natural and various diamino-modified kaolin at 30°C (clay 8 g/l; pH 5.7; initial Cu(II): 800 mg/l; initial Ni(II): 600 mg/l; initial Zn(II): 500 mg/l), where (a) Initial linear zone and (b) Final linear zone in adsorption processes.

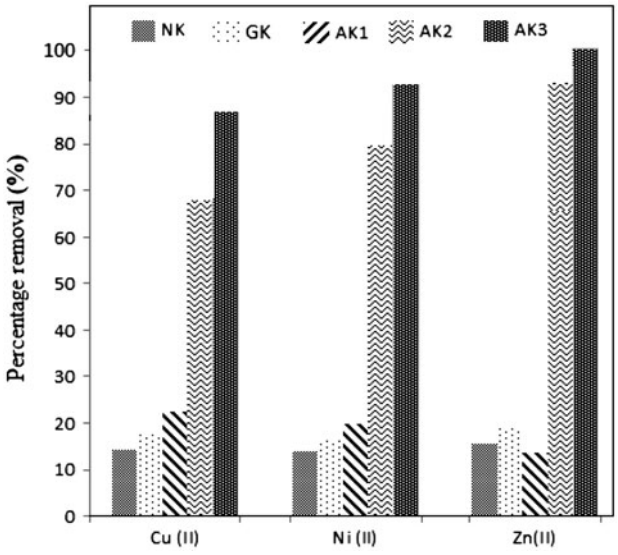

Fig. 9. Efficacy of natural and diamino-modified kaolin clays for removal of elevated concentrations Cu(II), Ni(II) and Zn(II) from aqueous medium at 30°C (clay 8 g/l; pH 5.7; time 120 min; initial metal ion concentration: 10,000 mg/l).

$min^{-0.5}$ for AK2 and 2.7 mg $g^{-1}min^{-0.5}$ for AK3) and Zn (II) (0.8 mg $g^{-1}min^{-0.5}$ for AK2 and 1.0 mg $g^{-1}min^{-0.5}$ for AK3) ions.

In this respect, the steeply sustainable metal ions uptakes onto kaolin/poly(glycine) composites as a function of Cu(II), Ni(II) and Zn(II) concentrations (Fig. 6) seem to be strongly correlated with the capability of those composites in interlayer expanding and uploading further ionic species within the micro- and meso- clay pore channels.

From the industrial point of view, it is bear to construct a diagram emphasizing the influence of interlayer expanding phenomena of amino-modified Sinai kaolinite onto the percentage removal of Cu(II), Ni(II) and Zn(II) ions from severe contaminated water (Fig. 9).

It is clearly evident that kaolin/poly(glycine) composites exhibit the best adsorption efficacy with grand applicability for exposure of hidden adsorption sites. Phenyl hydrazine modified kaolin/poly(glycine) composite shows 68, 80 and 93% removal for Cu(II), Ni(II) and Zn(II), respectively. Polyoxypropylenediamine modified kaolin/poly(glycine) composite spectacles 87, 93 and 98% removal for Cu(II), Ni(II) and Zn(II), respectively.

4. Conclusions

The natural Sinai kaolinite consisted of regular micro-sized platelets capable of being modified by glycine species and different aminated compounds. Glycine treated kaolinite was structurally disordered by gathering glycine molecules beyond kaolinite edges. Modifying glycine treated kaolinite via ethylenediamine led to retaining the Si–O–Si bridges linked with appearance of irregular flakes of lower surface area. Phenyl hydrazine modified glycine treated kaolinite exhibits a new sort of sites (peptide groups) originated from partial polymerization of glycine molecules developing kaolin/poly(glycine) composite. In accordance, the Si–O–Si, Si–O–Al as well Al–O–Al bridges were reformed and the surface properties become much closer to that of natural kaolinite. Modification of glycine treated kaolinite by polyoxypropylenediamine invented a long-range ordered and well- dimensioned kaolinite interlayers referring to *in situ* intensive glycine polymerization producing numerous polypeptides chains.

Natural kaolinite and their modified derivatives were able to remove Cu(II), Ni(II) and Zn(II) ions from severe contaminated water. The kaolinite modification approach was a significant impact in adsorption of metal ions. Copper, nickel and zinc adsorption profiles fitted Freundlish rather than Langmiur isotherms and followed both pseudo-first-order model through guest-host mass transfer diffusion and second-order kinetics via pore diffusion indicating advantageous adsorption of metal ions onto various accommodating active centres unevenly dispersed all over the clay sheet structure. The adsorption rate constants sequence onto natural Sinai kaolinite and their modified derivatives was Zn>Ni>Cu. Phenyl hydrazine and polyoxypropylenediamine kaolinite derivatives exhibited near 100% removal for Cu(II), Ni(II) and Zn(II) ions from aqueous medium due to their interlayer expandability resulting in revelation of hidden adsorption zones inside the micro- and meso-clay pore channels allowing thereby sustainable metal ion adsorption from severe contaminated water. The imperative results of the present work should attract the attention of both academic and industrial institutions and organizations towards the importance of Sinai deposits which need yet to be exploited.

References

[1] K.G. Bhattacharyya, S.S. Gupta, Adsorption of a few heavy metals on natural and modified kaolinite and montmorillonite: A review, Adv. Colloid Interface Sci. 140 (2008) 114–131.
[2] D. Ghosh, K.G. Bhattacharyya, Adsorption of methylene blue on kaolinite, Appl. Clay Sci. 20 (2002) 295–300.
[3] B.C. Raymahashay, A comparative study of clay minerals for pollution control, J. Geol. Soc. India 30 (1987) 408–413.
[4] K.A. Wierer, B. Dobias, Exchange enthalpies of H^+ and OH^- adsorption on minerals with different characters of potential-determining ions, J. Colloid Interface Sci. 122 (1988) 171–177.

[5] R.L. Frost, J.T. Kloprogge, J. Kristof, Encyclopedia of Surface and Colloid Science, Dekker, New York, NY, 2002.
[6] B. Singh, Geoenvironment: Proceedings of the 2nd Australia and New Zealand conference on environmental geotechnics, in: D. Smith, S. Fityus, M. Allman (Eds.), Australian Geochemical Society, Newcastle, 2001, pp. 77–93.
[7] S. Wang, Z. Nan, Y. Li, Z. Zhao, The chemical bonding of copper ions on kaolin from Suzhou, China, Desalination 249 (2009) 991–995.
[8] R.R. Rumer, M.E. Ryan (Eds.), Barrier Containment Technologies for Environmental Remediation, Wiley, New York, NY, 1995, pp. 49.
[9] H. Assameur, M. Boufatit, Contribution to the removal study of Co^{2+} ions by acid-activated clay from Maghnia (Algeria): Equilibrium and kinetic studies, Desali. Water Treat. 45 (2012) 315–323.
[10] A.K. Panda, B.G. Mishra, D.K. Mishra, R.K. Singh, Effect of sulphuric acid treatment on the physico-chemical characteristics of kaolin clay, Colloids Surf. A 363 (2010) 98–104.
[11] M. Lenarda, L. Storaro, A. Talon, E. Moretti, P. Riello, Solid acid catalysts from clays: Preparation of mesoporous catalysts by chemical activation of metakaolin under acid activation, J. Colloid Interface Sci. 311 (2007) 537–543.
[12] E. Mako, Z. Senkar, J. Kristof, V. Vagvolgyi, Surface modification of mechanochemically activated kaolinites by selective leaching, J. Colloid Interface Sci. 294 (2006) 362–370.
[13] K.G. Bhattacharyya, S.S. Gupta, Calcined tetrabutylammonium kaolinite and montmorillonite and adsorption of Fe(II), Co(II) and Ni(II) from solution, Appl. Clay Sci. 46 (2009) 216–221.
[14] T.S. Anirudhan, P.S. Suchithra, S. Rijith, Amine–modified polyacrylamide–bentonite composite for the adsorption of humic acid in aqueous solutions, Colloids Surf. A 326 (2008) 147–156.
[15] E.I. Unuabonah, B.I. Olu-owolabi, D. Okoro, K.O. Adebowale, Comparison of two-stage sorption design models for the removal of lead ions by polyvinyl-modified kaolinite clay, J. Hazard. Mater. 171 (2009) 215–221.
[16] H.A. Essawy, Poly(methyl methacrylate)-kaolinite nanocomposites prepared by interfacial polymerization with redox initiator system, Colloid Polym. Sci. 287 (2008) 795–803.
[17] C.R. Evanko, D.A. Dzombak, Influence of structural features on sorption of NOM-analog organic acids to goethite, Environ. Sci. Technol. 32 (1998) 2846–2855.
[18] J. Ikhsan, B.B. Johnson, J.D. Wells, M.J. Angove, Adsorption of aspartic acid on kaolinite, J. Colloid Interface Sci. 274 (2004) 1–5.
[19] ATSDR, Toxicological Profile for Copper, US Department of Health and Human Services Public Health Services (Agency for Toxic Substances and Disease Registry), Atlanta, GA, 2002.
[20] ATSDR, Draft Toxicological Profile for Nickel, US Department of Health and Human Services Public Health Services (Agency for Toxic Substances and Disease Registry), Atlanta, GA, 2003.
[21] C.G. Elinder, Zinc, In: L. Friberg, G.F. Nordberg, V.B. Vouk (Eds), Handbook on the Toxicology of Metals, second ed., Elsevier Science, Amsterdam, pp. 664–679, 1986.
[22] K.W. Sing, D.H. Everett, R.A.W. Haul, L. Moscou, R.A. Pierotti, J. Rouquerol, T. Siemieniewska, Reporting physisorption data for gas/solid systems with special reference to the determination of surface area and porosity, Pure Appl. Chem. 57 (1985) 603–619.
[23] H.D. Chapman, Cation exchange capacity, in: C.A. Black (Ed.), Method of Soil analysis. Part 2: Chemical and microbiological properties, American Society of Agronomy, Madison, WI, 1965, pp. 891–900.
[24] H. Kita, N. Henmi, K. Shimazu, H. Hattorin, J. Tanabe, Measurement of acid-base properties on metal oxide surfaces in aqueous solution, J. Chem. Soc. Farad. Trans. 77 (1981) 2451–2463.
[25] P. Zarzycki, F. Thomas, Theoritical study of the acid-base properties of the montmorillonite/electrolyte interface: Influence of the surface heterogeneity and ionic strength on the potentiometric titration curves, J. Colloid Interface Sci. 302 (2006) 547–559.
[26] X. Yang, Z. Sun, D. Wang, W. Forsling, Surface acid-base properties and hydration/dehydration mechanisms of aluminium hydroxides, J. Colloid Interface Sci. 308 (2007) 395–404.
[27] M.G.F. Rodrigues, Physical and catalytic characterization of smectites from Boa-Vista, Paraiba Brazil Ceramica 49 (2003) 146–150.
[28] M. Rozalén, P.V. Bardy, F.J. Huertas, Surface chemistry of K-montmorillonite: Ionic strength, temperature dependence and dissolution kinetics, J. Colloid Interface Sci. 333 (2009) 474–484.
[29] H.M.F. Freundlish, Über die adsorption in lÖsungen [Adsorption from solution], Zeitschrift fur Physikalische Chemie, Leipzig 57A (1906) 385–470.
[30] I. Langmuir, The adsorption of gases on plane surfaces of glass, mica and platinum, J. Am. Chem. Soc. 40 (1898) 1–39.
[31] K.R. Hall, L.C. Eagleton, A. Acrivos, T. Vermeulen, Pore- and solid diffusion kinetics in fixed-bed adsorption under constant pattern conditions, Ind. Eng. Chem. Fundam. 5 (1966) 212–223.
[32] Y.S. Ho, Removal of copper ions from aqueous solution by tree fern, Water Res. 34 (2003) 2323–2330.
[33] S. Lagergren, K. Sven, Theorie der sogenannten adsorption geloster stoffe [About the theory of so-called adsorption of soluble substances], Vetenskapsakad. Handl. 24 (1898) 1–39.
[34] M.M. Abou-Mesalam, Sorption kinetics of copper, zinc, cadmium and nickel ions on synthesized silico-antimonate ion exchanger, Colloids Surf. A 225 (2003) 85–94.
[35] Y.S. Ho, G. Mckay, Batch lead(II) removal from aqueous solution by peat: Equilibrium and kinetics, Trans. I Chem. E. 77B (1999) 165–173.
[36] Y.S. Ho, G. McKay, A comparative of chemisorption kinetic models applied to pollutant removal on various sorbents, Trans. Inst. Chem. Eng. 76B (1998) 332–339.
[37] W.J. Webber, J.C. Morris, Kinetics of adsorption of carbon from solution, J. Sanitary Eng. Div. Am. Soc. Civil Eng. 89 (1963) 31–63.
[38] G.E. Boyd, A.W. Adamson, Jr, L.S. Myers, The exchange adsorption of ions from aqueous solutions from organic zeolites Kinetics II, J. Am. Chem. Soc. 69 (1947) 2836–2842.
[39] M. Ugurlu, I. Kula, M.H. Karaoglu, Y. Arslan, Removal of Ni (II) ions from aqueous solutions using activated-carbon prepared from olive stone by $ZnCl_2$ activation, Environ. Prog. Sustainable Energy 4 (2009) 547–557.
[40] A. Gel, F.C.C. Assis, S. Albeniz, S.A. Korili, Removal of dyes from wastewaters by adsorption on pillared clays, Chem. Eng. J. 168 (2011) 1032–1040.
[41] M.B. Zbik, R.L. Frost, Micro-structure differences in kaolinite suspensions, J. Colloid Interface Sci. 339 (2009) 110–116.
[42] F.R. Farmer, Fast reactor safety, Ann. Nucl. Sci. Eng. 1 (1974) 255–264.
[43] J. Madejova, FTIR techniques in clay mineral studies, Vib. Spectrosc. 31 (2003) 1–10.
[44] C. Volzone, J.G. Thompson, A. Melnitchenko, J. Ortiga, S.R. Palethorpe, Selective gas adsorption by amorphous clay-mineral derivatives, Clays Clay Miner. 5 (1999) 647–657.
[45] R.Sh. Mikhail, N.M. Guindy, S. Hanafi, Adsorption of nitrogen on Vermicutite: Nitrogen t-curves on low heat surfaces, J. Chem. (1973) 53–66, special issue "Tourky".

[46] S.S. Gupta, K.G. Bhattacharyya, Immobilization of Pb(II), Cd (II) and Ni(II) ions on kaolinite and montmorillonite surfaces from aqueous medium, J. Environ. Manage. 87 (2008) 46–58.
[47] N.K. Daud, B.H. Hameed, Acid Red 1 dye decolorization by heterogeneous Fenton-like reaction using Fe/kaolin catalyst, Desalination 269 (2011) 291–293.
[48] M. Jiang, X. Jin, X. Lu, Z. Chen, Adsorption of Pb(II), Cd(II) Ni(II) and Cu(II) onto natural kaolinite clay, Desalination 252 (2010) 33–39.
[49] E.I. Unuabonah, K.O. Adebowale, B.I. Olu-owolabi, L.Z. Yang, L.X. Kong, Adsorption of Pb(II) and Cd(II) from aqueous solutions onto sodium tetraborate-modified kaolinite clay: Equilibrium and thermodynamics studies, Hydromettallurgy 93 (2008) 1–9.
[50] Ö. Yavuz, Y. Altunkaynak, F. Guzel, Removal of copper, nickel, cobalt and manganese from aqueous solution by kaolinite, Water Res. 37 (2003) 948–952.
[51] K. Li, Z. Zheng, J. Feng, J. Zhang, X. Luo, Adsorption of p-nitroaniline from aqueous solutions onto activated carbon fiber prepared from cotton stalk, J. Hazard. Mater. 166 (2009) 1180–1185.
[52] A. Bhatnagar, A.K. Jain, A.K. Minocha, S. Singh, Removal of lead ions from aqueous solutions by different types of industrial waste materials: Equilibrium and kinetic studies, Sep. Sci. Technol. 41 (2006) 1881–1892.
[53] V.K. Gupta, A. Rastogi, V.K. Saini, N. Jain, Biosorption of copper(II) from aqueous solutions by Spirogyra species, J. Colloid. Interface Sci. 296 (2006) 59–63.
[54] K.O. Adebowale, E.I. Unuabonah, B.I. Olu-Owolabi, Kinetic and thermodynamic aspects of the adsorption of Pb^{2+} and Cd^{2+} ions on tripolyphosphate-modified kaolinite clay, Chem. Eng. J. 136 (2008) 99–107.
[55] S. Coruh, F. Geyikci, Adsorption of copper ions on montmorillonite and sepiolite clays: Equilibrium and kinetic studies 45 (2012) 315–360.